Article

Not peer-reviewed version

Passive Films Formed on Fe and Ni Based Alloys in an Alkaline Medium: An Insight into Complementarities between Electrochemical Techniques and Near-Field Microscopies (AFM/SKPFM)

Noureddine Benaioun , Nasreddine Moulayat , Noureddine Hakiki , Hanene Ramdane , Emmanuel Denys , Alban Florentin , Kouider Driss Khodja , Mohamed Heireche , Jean Luc Bubendorff *

Posted Date: 28 September 2023

doi: 10.20944/preprints202309.1931.v1

Keywords: Stainless steel; nickel-based alloy; Cyclic voltammetry; Electrochemical impedance spectroscopy; Atomic force microscopy; SKPFM

Article

Passive Films Formed on Fe and Ni Based Alloys in an Alkaline Medium: An Insight into Complementarities between Electrochemical Techniques and Near-Field Microscopies (AFM/SKPFM)

N. E. Benaioun [1,2,*], N. Moulayat [2], N. E. Hakiki [2], H.Ramdane [2], E. Denys [1], A. Florentin [1], K. Driss Khodja [3] and M. M. Heireche [4], J.L. Bubendorff [1*]

[1] Université de Strasbourg(UdS)-Université de Haute Alsace (UHA), Institut de Science des Matériaux de Mulhouse (IS2M), UMR 7361 du CNRS, 3b rue Alfred Werner, 68093 Mulhouse, France.
[2] Université d'Oran I Ahmed Benbella, Laboratoire de Physique des Couches Minces et Matériaux pour l'Electronique (LPC2ME), BP 1524, El M'Naouer, 31000 Oran, Algéria.
[3] Université d'Oran I Ahmed Benbella, Laboratoire de Théorie et de Simulation des Matériaux, BP 1524, El M'Naouer, 31000 Oran, Algéria.
[4] Ecole national supérieure d'Oran, BP 1063 SAIM MOHAMED,31003 ORAN,Algéria.
* Correspondence: jean-luc.bubendorff@uha.fr; benaioun.noureddine@gmail.com

Abstract: This study presents a combined electrochemical impedance spectroscopy (EIS) and atomic force microscopy (AFM) and Scanning Kelvin Probe Force Microscopy(SKPFM) investigation on the natural passivation process of stainless steels (AISI 316 and AISI 304) and nickel-based alloy (INCONEL 600) as a function of immersion time in an alkaline medium (pH = 13). EIS measurements show an increase in the resistance of the film with increasing immersion time in the electrolyte. After 3 days of immersion, for the three alloys, the films formed constitute an effective barrier to the dissolution of the alloys as shown by AFM and SKPFM. The oxide film growth on each substrates is only influenced by trenches formed during the polishing step and don't depend on the chemical composition.

Keywords: stainless steel; nickel-based alloy; cyclic voltammetry; electrochemical impedance spectroscopy; atomic force microscopy; SKPFM

1. Introduction

The discovery of reinforced concrete at the end of the 19th century, allowed the civil engineering field to make remarkable advances. Indeed, it made it possible to achieve more complex structures and increased their lifetime. This can be possible thanks to the fact that the steels embedded in the concrete are surfaced with a passive film which will protect it against the corrosive agents. The passive film is the result of the interaction between the steels and its direct environment, for example, the exposure of iron and steel to an alkaline environment promotes the formation of this protective passive film [1-7]. However, several factors such as humidity, temperature [3, 8], pH and halogens (chloride ions) may lead to the destruction of the protective passive films, reducing the lifetime of reinforced concrete structures. The physical and electrochemical properties of passive film depend mainly on both the environment (temperature, pressure, pH,) and the chemical composition of the steel used [9,10]. The replacement of standard steels by more resistant alloys became crucial. Among these alloys, stainless steels invented by Monnartz [11], have the ability to form passive films that will occur by very complex training processes. These processes are not fully understood and are subjected to many controversies but stainless steels remains a good solution for engineering purposes instead of traditional carbon steel[10]. Recently it has been shown that the industrial water polluant named Red Mud (RM) had positive effects on the corrosion resistance of steel in concrete, which was more pronounced in the presence of chlorides which is a promising new way for the cement industry

to reduce their environmental impact [12. Moreover, other alloys have been developed for various application fields such as nickel based alloys [13] that are used for equipping chemical and nuclear power plants especially steam generators in pressurized water reactors (PWR). However, the literature is less abundant on nickel-based alloys exposed to very alkaline media at room temperature, which is why we have studied it in a previous paper [14] and now in this paper we compare the behavior of INCONEL 600 with that of stainless steels.

In an alkaline medium, the studies of the films formed on iron showed the presence of magnetite Fe_3O_4 which will oxidize into hematite Fe_2O_3 [15, 16]. Other investigations have also been conducted on Fe-Cr alloys, and revealed the presence of Cr (III) oxy-hydroxide in the inner layer of the film [17, 18]. For stainless steels, it has been demonstrated that the oxide has a bilayers structure: an outer layer very enriched in iron oxide and hydroxide is in contact with the electrolyte, and an internal layer enriched with chromium oxide is in contact with the alloy [19-20]. Both layers forming the electrical equivalent of an n-p junction behaved like a diode stopping the future diffusion of corrosives chemical species and so forming an effective protection layer against corrosion [21]. Given these properties, the stainless steels are more reliable for the construction of complex structure in hostile environments.

Electrochemical impedance spectroscopy (EIS) is one of the most widely used techniques in recent decades to identify the different processes occurring during the growth of passive films [10,22-26]. It is a non-destructive technique that makes it possible to simulate the behavior of a given system (metal, film, solution) by an equivalent electrical circuit (EEC) without altering the composition and the structure of the studied films. The components of the EEC (resistances, capacitors ...) correspond to the different processes (double electric layer, adsorption, oxidation-reduction reactions ...) taking place at the electrode/electrolyte interface. According to Macdonald [27] the obtained circuit is not a model but an analogy because the same experimental data can be expressed in different equivalent circuits.

Local near-field imaging techniques like Atomic Force Microscopy (AFM), Scanning Kelvin Probe Force Microscopy (SKPFM) allow the observation of the inhomogeneities of surfaces at the nanometric scale. For example, it can reveal the localization of porosity areas on the film or passivity breaks which would make the material subjected to corrosion. L. Veleva et al. [28] have studied passive films formed by cyclic voltammetry on AISI 316 in solutions of $Ca(OH)_2$ and of cement extract by AFM. They observed by AFM a morphology difference between the two films obtained: the film formed in saturated $Ca(OH)_2$ is rough, crystalline and non-homogeneous whereas the passive layer formed in the cement extract solution is homogeneous and covers the metal surface completely. More recently, in 2017, Y. Li et al [29] studied the growth of passive films on carbon steels by EIS and confirmed there EIS results by AFM measurements. Therefore, we decide to correlate the resistance of passive films formed on Ni-based alloys (Inconel) and stainless steel with its surface topography to better understand the passivation process.

In the present study, we started by investigating films formed by cyclic voltammetry (CV) on AISI 304 and AISI 316 stainless steels and INCONEL 600 nickel-based alloy. To do so, we used the EIS to determine the most protective films in an alkaline solution at pH = 13 simulating the environment of reinforced concrete. In the second part of this work, we studied the evolution of spontaneously formed films for the three alloys depending on the immersion time. We use EIS and AFM microscopy to provide additional information on the growth of passive films on two stainless steels (AISI 304 and AISI 316) and a nickel-based alloy (Inconel600) in an alkaline environment simulating reinforced concrete. For this last point, we focused on the spontaneous formation of films in order to better simulate actual conditions of use of these materials, since CV modifies the chemical composition of the outer layer and its thickness. We notice that all the materials could be simulated by the same equivalent electric circuit what indicate that may be the passivation process is approximately the same whatever the substrate is.

2. Materials and Methods

2.1. Materials

Preprints (www.preprints.org) | NOT PEER-REVIEWED | Posted: 28 September 2023 doi:10.20944/preprints202309.1931.v1

In this work, the stainless steels and the nickel-based alloy were provided by Goodfellow, their chemical composition is given in table 1.

Table 1. Chemical composition of stainless steels (AISI 304, AISI 316) and INCONEL 600.

Eléments	*Cr*	*Ni*	*C*	*N*	*Si*	*Mn*	*Mo*	*Cu*	*S*
AISI 304	*18*	*10*	*0.053*	*0.04*	*0.48*	*1.42*	*0.39*	*0.14*	*0.024*
AISI 316	*18*	*10*	*0.053*	*0.025*	*0.75*	*1.24*	*3.0*	*0.2*	*0.027*
Eléments	*Cr*	*Fe*	*C*	*N*	*Si*	*Mn*	*P*	*Ti*	*S*
Inconel 600	*29*	*10*	*0.033*	*0.007*	*0.28*	*0.65*	*0.007*	*0.28*	*0.003*

The samples (size: 1 x 1 cm^2) were embedded in an epoxy resin, then abraded with wet SiC paper of decreasing grit size (1000, 2400 and 4000) and polished with a diamond paste (particle size: 3 and 1 μm). The used polisher is marketed by PERSI compagny, allowing the control of the rotation speed (ω in rad/s), the time (t in s) and the force (F in N) applied on the sample. The different polishing steps were controlled by an optical microscope. After polishing, the sample was extracted from the epoxy resin and then rinsed in ultrasound baths with acetone, ethanol and deionized water and dried by air. The final substrate surface was checked for the three alloys by AFM as shown in Figure 1. Low roughness surfaces (RMS: AISI 304 = 3.0 ±0.1 nm, AISI316=2.70 ±0.1 nm, INCONEL 600 = 2.8 ±0.2 nm) were obtained. Since the roughness values are very close together, we could not distinguish the surface topography from one sample compared to another. As can be seen on Figure 1, proper polishing grooves appear parallel at this micrometer scale. To obtain a physical parameter other that the RMS roughness to characterize each substrate, we calculate the self-correlation function G defined as:

$$G(k_1,k_2)=\sum_{i=1}^{512}\sum_{j=1}^{512}h(i,j)\times h(i+k_1,j+k_2) \quad (1)$$

From the geometrical point of view, this function probes the correlation between the original image and an image shifted by a distance k_1 (k_2) in the x (y) direction with respect to the center of the original image. This function reaches always its maximum at the center of its image and the shape of the central peak give access to the grains mean geometrical shape [14]. If there is a periodicity in the image, it will also appear in the self-correlation image. In our case, trenches due to polishing are parallel and separated by a mean distance l that we can determine using the sections associated to each self correlation image. The sections show maximums corresponding to the periodicity due to parallel trenches. By measuring the distance between two maxima, we obtain the characteristic parameter l corresponding to the mean distance separating two trenches (see section of imageA1on figure 1 for example). To obtain a more precise value of l, we measure the distance between 10 maximums and divided the measured value by 10 to obtain l for each substrate. We obtain l =110±10 nm for the Inconel 600 substrate and l =193±20 nm for AISI304 and l =83±15 nm for AISI316 substrates. To conclude, the several lengths l obtained are different for each substrate and l is a parameter that allow to characterize the differences between the surface topographies due to our polishing technique before the passivation process starts.

Preprints (www.preprints.org) | NOT PEER-REVIEWED | Posted: 28 September 2023 doi:10.20944/preprints202309.1931.v1

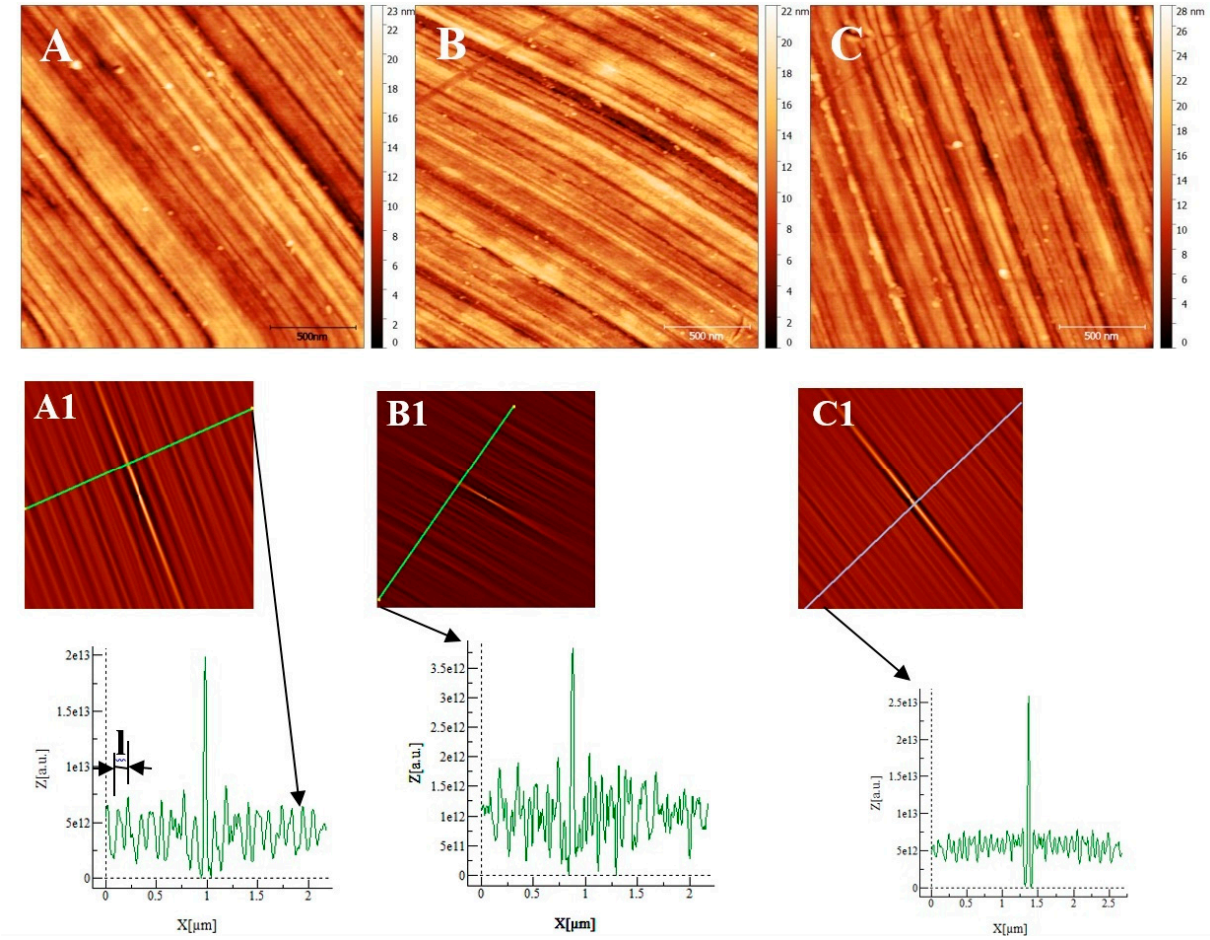

Figure 1. Atomic Force Microscopy image (2 µm x 2 µm) of the substrate after polishing: (A) AISI 304. (B) AISI 316. (C) INCONEL 600. (A1), (B1) and (C1) are self-correlation images calculated using respectively images A, B and C as input with typical cross-sections allowing to determine the average distance named l between two trenches resulting from the polishing steps.

2.2. Electrochemical measurements.

All measurements were conducted in a 0.1M NaOH solution at pH = 13, to simulate the interstitial electrolyte of concrete pores. The electrochemical experiments were performed at room temperature in a classical electrochemical cell with three electrodes. We used as a reference a saturated calomel electrode (SCE, E^0 = +0.24V versus the Saturated Hydrogen Electrode (SHE)), as a counter electrode we used a platinum electrode. The working electrodes have been developed with the materials studied, i.e. AISI 304, AISI 316 and INCONEL 600. All the electrochemical measurements were carried out using a potenstiotat from Princeton Applied Research (versaStat 4).

We used Cyclic Voltammetry (CV) to determine the redox processes on the passive films generated by the application of the potential sweep. The range of potential selected extends from the evolution of hydrogen (-1.4 V vs SCE) to the evolution of oxygen (+0.6 V vs SCE). In order to obtain thick passive films, we performed 12 cycles with a scanning rate of 25 mV/s. These experimental conditions allowed the identification of the redox processes which tended to decrease and those which tended to increase with the numbers of the scanning cycles in potential [30].

Passive films formed by CV and spontaneously formed films were studied and compared using electrochemical impedance spectroscopy (EIS). These measurements were performed after the OCP (Open Circuit potential) was stable. The amplitude of the tension applied was 10 mV and the scanning frequency was ranged between 100 kHz and 5 mHz. The working electrodes were not cathodically polarized to remove the native oxides (formed in air) in order to stay in conditions close to those where the alloys evolve in reinforced concrete.

 doi:10.20944/preprints202309.1931.v1

2.3. Atomic force microscopy (AFM).

The AFM images were realized with an AFM provided by Brucker ((multimode design, Nanoscope V electronic). The AFM in tapping mode was used to monitor the evolution of the topography during the different immersion times. The principle and the different modes of acquisition of the AFM images are widely explained and detailed in the litterature [31-33]. For SKFM images, we use PtIr coated tapping mode Si tips provided by Brucker with a resonant frequency around 75 kHz and a stiffness constant around 3 Nm^{-1}. Our experimental procedure to obtain a SKPFM image has been described in a previous paper [21].

3. Results and discussion

3.1. Films formed by cyclic voltammetry.

In this section we have formed and characterized the passive films on AISI 304 and AISI 316 stainless steels as well as on INCONEL 600. The voltammograms obtained (Fig. 2A) for AISI 304 and AISI 316 are comparable and are in agreement with the literature results [28, 34-37]. For the two materials, there are clearly three zones:

a) The zone I: extended from -1.4 to -0.56 V vs SCE called pre-passivity zone is the typical region of iron activity.
b) The zone II: extended from -0.56 to 0 V vs SCE is the region where a stable passive film covering the surface of the alloys is formed (passivation).
c) Zone III: extended from 0 to 0.6 V vs SCE, called zone of transpassivity is the region where the oxidation reduction processes of alloying elements occur (Cr, Ni, ...). It is in this zone where the water decomposes causing an evolution of oxygen which conduct on the voltammograms to a strong increase in the anodic current density.

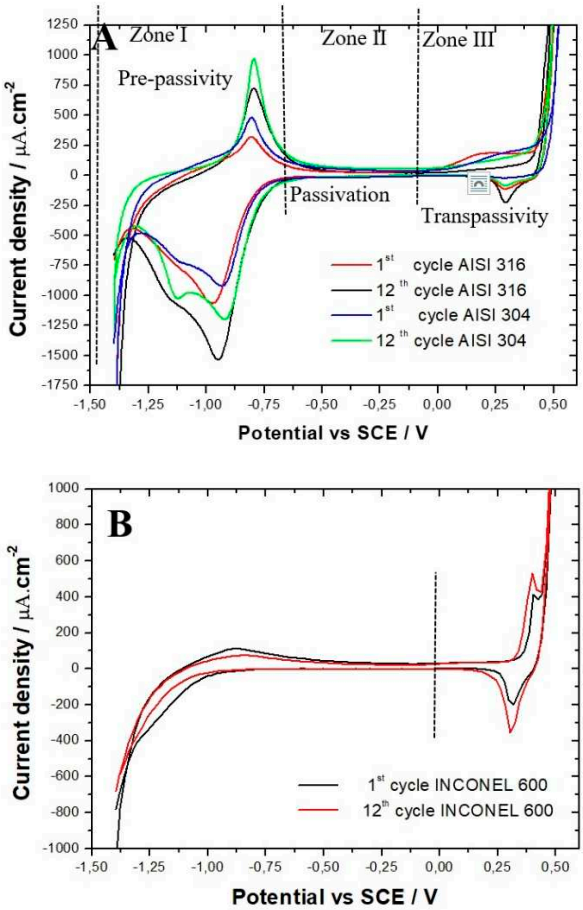

 doi:10.20944/preprints202309.1931.v1

Figure 2. Cyclic voltammograms (1 st and 12 th cycles) obtained in 0.1 M NaOH solution. Potential range: -1.4 to 0.5 V vs SCE. Scanning rate:dE/dt = 25 mV/s. (A) AISI 316 and AISI 304 samples. (B) INCONEL 600.

The zone I corresponds to the zone of iron activity, the presence of an oxidation peak is observed at about -0.8 V vs SCE, which is essentially due to the formation of the magnetite Fe_3O_4 [34, 37-39] as shown in the following equations.

$$3Fe(OH)_2 + 2OH^- \leftrightarrow Fe_3O_4 + 4H_2O + 2e^- \quad (2)$$

$$3FeO + 2OH^- \leftrightarrow Fe_3O_4 + H_2O + 2e^- \quad (3)$$

Magnetite is a mixed oxide which results mainly from the oxidation of Fe^{2+} to Fe_3O_4 composed by Fe^{2+} and Fe^{3+} [36-37]. As can be seen in Fig. 2A., for both steels, an increase of the peak intensity is observed with the increase in the number of cycles. The density of the anode current corresponding to the magnetite formation is greater for the AISI 304 than for the AISI 316 (975 µA/cm²; 713µA/cm² respectively). The presence of a less intense oxidation peak for AISI 316 is due to the presence of in the chemical composition of the AISI 316 alloy. The molybdenum promotes the inner layer enrichment by the chromium oxide film Cr_2O_3 [37, 39-40] with an insulating behavior that blocks the movement of iron ions through the film. As indicated in their work, C. M. Abreu et al. [37] showed that a higher intensity of the oxidation peak leads to a thicker film. Therefore, the films formed on AISI 304 are thicker than those formed on AISI 316. Beyond the peak of magnetite formation there is a sudden drop in anodic current density which is characteristic of a transition from an active state of stainless steels dissolution to a state of passivation. The intensity of the reduction peaks at -0.97 and -1.12 V vs SCE increases with increasing numbers of cycles. The processes that occurs at these peaks is not well understood. Thus, some authors agree that these peaks correspond to the reduction of Fe^{3+} to Fe^{2+}. Other authors indicate that this would be the reduction of Ni_3O_4 to NiO and NiO to Ni metal. In their studies on stainless steels (AISI 304 and AISI 316) L. Freire et al [34] suggest that there is an overlap between the reduction of nickel oxides (Ni_3O_4 to NiO and NiO to Ni metal) and the reduction of iron oxides (Fe_3O_4 to Fe^{2+}).

In zone II, the anode current density is constant and low (residual current density). The existence of this potential domain (domain of passivation) where the current density is very small provide the idea that in an alkaline medium the films on the surface of the alloys acts as a barrier separating the stainless steel from the electrolyte [38].

In the zone III also called the transpassivity region, important changes are observed. Figure 2A shows an oxidation peak in the region of chromium activity at about 0.23 V vs SCE which corresponds to the chromium oxidation process: Cr^{3+} / Cr^{6+} [34-36, 38, 41]. It should also be noted that the intensity of the chromium oxidation peak decreases with the increase of the number of cycles suggesting the progressive formation of an isolating oxide layer like Cr_2O_3, which decrease the reactivity of the passive layer. At more positive potentials than the peak oxidation of chromium, we observe an intense increase in the current density due to water decomposition generating an evolution of oxygen [38]. The reduction peak at 0.29 V vs SCE whose intensity increases with cycles corresponds to the reduction process Ni^{2+} / Ni^{3+} [35-36].

The voltammograms (Fig. 2B) obtained on the INCONEL 600 are similar to those found in the litterature [39-43]. However, they are different from those obtained on the AISI 304 and AISI 316 (Fig. 2A). Figure 2B shows an intensity increase of the oxidation peak at 0.39 V vs SCE and of the reduction peak at 0.30 V vs SCE with increasing number of cycles. These two peaks are attributed to the transition process from $Ni(OH)_2$ to NiO(OH) and conversely [42, 43]. The intensity of the oxidation peak of Fe^{2+} to Fe_3O_4 at -0.86 V vs SCE tends to decrease [37]. On our voltammograms, we do not find any chromium oxidation peak. Nevertheless, XPS measurements performed by C.M. Abreu et al. [37] on films formed by cyclic voltammetry on the surface of nickel base alloys in an alkaline medium revealed the presence of chromium Cr^{3+} in the film.Zone 1 of the voltammograms showed that the films formed on AISI 304 are thicker than those formed on AISI 316. However, the

Preprints (www.preprints.org) | NOT PEER-REVIEWED | Posted: 28 September 2023 doi:10.20944/preprints202309.1931.v1

fact that they are thicker does not necessarily mean that they are more protective. The values of the average residual current measured for AISI 316 and AISI 304 stainless steels are reported in Table 2. In the first cycle it can be seen that the average residual current for AISI 316 (11.57 µA/cm²) is lower than that of AISI 304 (14.55 µA/cm²), suggesting that the passive film formed on AISI 316 is more protective than the one formed on AISI 304. This trend is confirmed during the cycles. For example, in the twelfth cycle, there is a decrease in the average residual current for the two alloys (3.95 µA/cm² for AISI 316 and 6.88 µA/cm² for AISI 304). The barrier properties of the films are improved with the increase in the number of cycles. These results are consistent with those found in the literature [38]. The mean residual current measured for the INCONEL 600 after twelve cycles (4.86 µA / cm²) was found between the one measured on AISI 304 and on AISI 316. This suggests that the film formed on INCONEL 600 in a simulated concrete environment at ambient temperature is more resistant than those formed on AISI 304 but less than those formed on the AISI 316.

Table 2. The residual current of the passivity domain of both stainless steels (AISI 304 and AISI 316) and INCONEL 600 determined form the cyclic voltammograms.

	AISI 304	AISI 316	INCONEL 600
Courant résiduel (µA.cm^{-2}) cycle 1	14.55	11.57	15.60
Courant résiduel (µA.cm^{-2}) cycle 12	6.88	3.95	4.86

To confirm these results, we used electrochemical impedance measurements to determine the overall system impedance for the three alloys after CV in an alkaline solution of NaOH at pH = 13. Measurements were made from 100 KHz to 2.5 MHz. The analysis of the Bode diagram (see Fig. 3) shows the same trend for the three alloys. At low frequencies, the impedance measured for AISI 316 was higher than the one measured on INCONEL 600 which displayed an higher impedance than AISI 304. These data's confirm the previous results obtained with the average residual current measurements. Taken together, these elements seem to suggest that the INCONEL 600 which is an alloy generally used in critical environments, is less efficient than AISI 316 at room temperature in an environment simulating reinforced concrete.

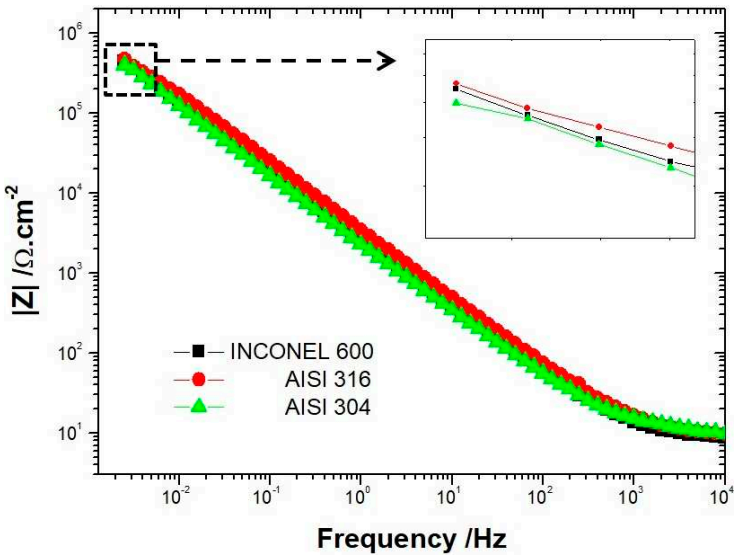

Figure 3. Bode plots (log|Z|) of AISI 304, AISI 316 and INCONEL 600 in NaOH solution after cyclic voltammograms.

3.2. Spontaneous growth of passive films on stainless steels and INCONEL 600.

3.2.1. Electrochemical impedance spectroscopy.

Preprints (www.preprints.org) | NOT PEER-REVIEWED | Posted: 28 September 2023 doi:10.20944/preprints202309.1931.v1

Evolution of the Nyquist diagrams as a function of the immersion time in the solution simulating reinforced concrete for the three alloys are shown in Figure 4. For the three alloys, the capacitive loop reported has a diameter that increases with the exposure time, meaning that the resistance of the passive films formed increases with the immersion time, which is in agreement with the literature [9, 26, 44]. The authors suggest that the steady state of the steels exposed to alkaline media is well established after 3 days of immersion. This is the reason why we chose to collect EIS data's during this time laps [9, 26]. For both AISI 304 and AISI 316, the impedance measurements performed show that the capacitive loop has a linear behavior at low frequencies range after 72 hours of immersion. Suggesting that the film formed is stable and protective. This tendency is less clear for the INCONEL 600, meaning that the amplitude of the capacitive loops is less than that of the stainless steels AISI 304 and AISI 316. This indicates the films formed on INCONEL 600 in an alkaline medium at pH = 13 are less effective than those formed on stainless steels.

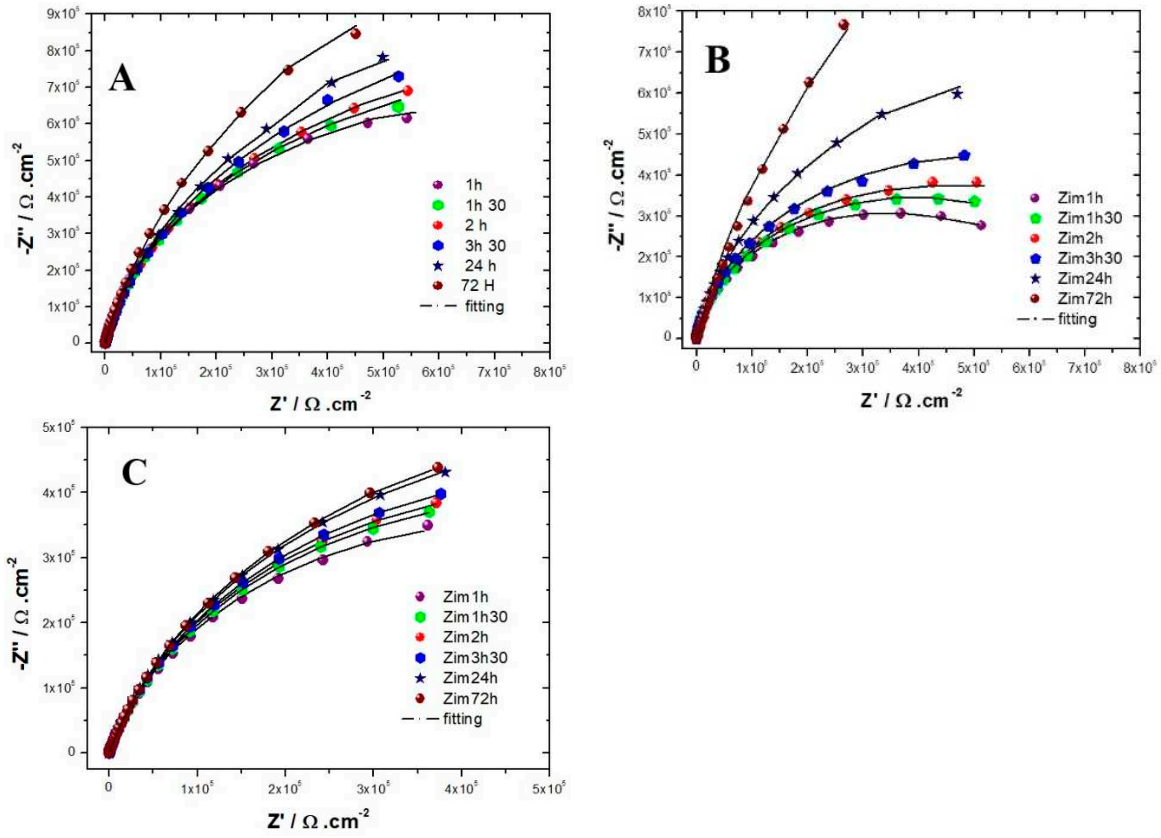

Figure 4. Experimental and simulated Nyquist plots as a function of immersion time obtained for (A) AISI 316. (B) AISI 304. (C) INCONEL 600 in a NaOH (pH=13) solution at OCP (from100 kHz down to 5 mHz).

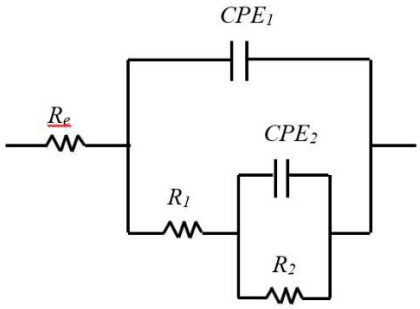

Figure 5. Equivalent circuits with two characteristic times constant used to represent the impedance behavior of the film/electrolyte interface as a function of immersion time.

Preprints (www.preprints.org) | NOT PEER-REVIEWED | Posted: 28 September 2023 doi:10.20944/preprints202309.1931.v1

In this study, the results of the EIS measurements were exploited using an equivalent electrical circuit EEC. Several equivalent circuits have been tested and the circuit depicted in Figure 5 with two times constant was selected to fit the experimental data because it gave the more reliable results and allowed to simulate EIS data's with the same circuit for all 3 samples what allow to compare them easily. This circuit was applied in other studies to describe passivation for AISI304 [44], AISI316 [26] and Inconels [45], which is why it seems for us adapted to our electrochemical system. The EEC fitting parameters are described in Table 3, 4 and 5. The use of EEC suggests that the passive film contains porosities in which the electrolyte penetrates [39, 46]. The expression of the total impedance of the EEC is given by Equation 4. The half circles observed on the Nyquist diagrams are more or less flattened, which is explained by the non-ideality (roughness) of the electrodes surface. So, it would be better as shown on Equation 4 to replace the pure capacities of the circuit by constant phase elements CPE: CPE_1 with a capacitance C_1 and an exponent α_1 and CPE_2 with a capacitance C_2 and an exponent α_2. The properties of the CPE depend on the values of α. When α is equal to 1 the CPE behaves as a pure capacity and when α is equal to 0.5 the CPE behaves like an impedance of Warburg (diffusional control of the formation of the film).

$$Z(\omega) = R_e \frac{R_1}{\frac{1}{1+\left(Z_2(\omega)/R_1\right)} + \left(j\omega R_1 C_1\right)^{\alpha_1}} \qquad (4)$$

$$Z_2(\omega) = \frac{R_2}{1+\left(j\omega R_2 C_2\right)^{\alpha_2}}$$

In our case, the literature suggests that the first time constant is associated with the charge transfer process where R_1 is the charge transfer resistance and CPE_1 is the capacitance of the double layer at high frequencies. At low frequencies, the second time constant is associated to the oxidation-reduction process which takes place in the passive film. C_2 is associated to the capacitive behavior of the film and R_2 is linked to the resistance of the oxidation-reduction process [1, 26].

Tables 3 and 4 group together the values of the equivalent circuit parameters in the case of stainless steels. For AISI 316, the values of α_1 vary between 0.94 and 0.92 while those of α_2 vary between 0.84 and 0.82. For AISI 304, α_1 varies between 0.95 and 0.94 and α2, between 0.87 and 0.86. The values obtained for α are very close to 1 for both types of stainless steels, in agreement with the literature [22] CPE can be assimilated to pure capacitors (CPE≈C). Like stainless steels, in the case of Inconel 600, CPE can also be assimilated to pure capacitors (α_1 and α_2 are close to 1 Cf. table 5).

Table 3. Best fit parameters for the impedance spectra obtained on AISI 316 in NaOH solutions after OCP stabilization.

	1h	1h30	2h	3h30	24h	72h
CPE_1 ($10^{-4}\Omega^{-1}cm^{-2}s^{\alpha}$)	34.0	18.2	15.1	13.8	10.5	9.2
Error %	0.36	1.90	1.43	1.75	0.89	1.11
α_1	0.94	0.93	0.93	0.93	0.92	0.93
Error %	0.25	2.40	0.27	0.21	2.14	0.28
R_1 ($k\Omega/cm^2$)	17.3	39.2	35.4	41.3	48.1	69.7
Error %	4.78	3.25	0.73	4.52	6.14	4.22
CPE_2 ($10^{-4}\Omega^{-1}cm^{-2}s^{\alpha}$)	87.1	78.0	61.4	32.2	25.4	28.6
Error %	3.06	5.21	2.04	4.75	3.93	0.48
α_2	0.84	0.84	0.83	0.84	0.82	0.84
Error %	1.93	1.26	2.39	4.5	5.2	2.89
R_2 ($k\Omega/cm^2$)	459.1	568.2	698.0	754.8	878.4	993.9
Error %	5.25	4.11	3.70	1.39	3.24	5.01

Preprints (www.preprints.org) | NOT PEER-REVIEWED | Posted: 28 September 2023 doi:10.20944/preprints202309.1931.v1

Table 4. Best fit parameters for the impedance spectra obtained on AISI 304 in NaOH solutions after OCP stabilization.

	1h	1h30	2h	3h30	24h	72h
CPE_1 ($10^{-6}\Omega^{-1}cm^{-2}$ s^{-n})	22.1	18.1	17.9	16.8	10.1	7.9
Error %	3.10	0.97	2.80	0.93	0.82	2.71
α_1	0.95	0.95	0.95	0.94	0.94	0.94
Error %	0.13	0.25	0.14	0.21	0.29	0.98
R_1 ($k\Omega/cm^2$)	28.6	29.1	34.7	52.1	58.3	86.0
Error %	6.30	2.91	0.27	4.94	1.97	2.39
CPE_2 ($10^{-6}\Omega^{-1}cm^{-2}$ s^{-n})	42.2	21.9	15.2	13.4	11.4	9.67
Error %	5.87	6.01	1.35	0.90	2.31	1.74
α_2	0.87	0.87	0.86	0.86	0.87	0.87
Error %	1.32	0.90	1.7	2.3	0.1	0.4
R_2 ($k\Omega/cm^2$)	251.2	342.2	380.1	412.8	570.4	749.9
Error %	0.8	5.12	1.84	3.30	2.24	2.62

Table 5. Best fit parameters for the impedance spectra obtained on INCONEL 600 in NaOH solutions after OCP stabilization.

	1h	1h30	2h	3h30	24h	72h
CPE_1 ($10^{-6}\Omega^{-1}cm^{-2}$ s^{-n})	32.4	28.2	26	25.4	23	23.0
Error %	1.51	2.45	1.16	3.50	1.19	0.31
α_1	0.96	0.96	0.97	0.96	0.97	0.96
Error %	2.32	2.21	1.90	1.10	0.12	0.55
R_1 ($k\Omega/cm^2$)	17.3	20.1	42.5	76.4	97.8	120.3
Error %	0.85	5.68	2.36	1.19	7.65	1.33
CPE_2 ($10^{-6}\Omega^{-1}cm^{-2}$ s^{-n})	17.3	25.0	19.8	15.1	6.1	1.9
Error %	4.81	2.52	1.95	0.87	1.25	3.10
α_2	0.78	0.79	0.78	0.77	0.78	0.78
Error %	4.87	1.61	0.58	2.1	0.12	2.44
R_2 ($k\Omega/cm^2$)	280.7	320.1	430.2	470.4	522.3	510.5
Error %	0.98	4.54	5.55	3.74	3.85	2.19

For all three alloys, the values obtained by fitting CPE_1 (between 34.0 and 7.910^{-6} $\Omega^{-1}cm^{-2}$ s^{-n}) indicate that it can be assimilated to the capacity of the double layer. The increase for both stainless steels of the charge transfer resistance R_1 from 20.4 to 69.7 $k\Omega/cm^2$ for AISI 316, and from 28.6 to 81.1 $k\Omega/cm^2$ for AISI 304 with the increase of the immersion time, shows the increasing difficulty that the charge transfer process can encounter to be achieved. Thus, this hypothesis seems to be relatively well in line with the increase in resistance R_2 from 459.1 to 993.9 $k\Omega/cm^2$ for AISI 316 and from 251.2 to 749.9 $k\Omega/cm^2$ for AISI 304 (fig 6). The CPE_2 and R_2 parameters associated with the redox process that can take place within the film are affected by the immersion time. One of the possible reactions, which contributes to this process is represented by the following equation [26]:

$$Fe3O4 + OH- + H2O \leftrightarrow 3FeOOH + e- \quad (5)$$

As expected, the barrier properties of passive films increase with immersion time [9, 26]. For stainless steels, it is recognized in the literature that the increase in film resistance is due to the enrichment of chromium oxide. The inner layer of the film adhering to the substrate is composed by Cr_2O_3 oxide which has the properties of an insulator. The outer layer is essentially composed by iron oxide. It has been shown by Addari et al [9] that the aging of the films in alkaline environments gives rise to a predominance of the oxide Fe_2O_3.

Compared to AISI 304, for example, INCONEL 600 does not show much difference between the spectra acquired at t=1h and t=72h. The linear character of the capacitive loop at low frequencies at t= 24h and t= 72h is less clear than for the other two alloys, suggesting that the films formed naturally on INCONEL 600 in alkaline media would be less effective. This is because the value of the polarisation resistance R_p (which is obtained by extrapolation of the Nyquist curve) at t=72h for INCONEL 600 is lower than for stainless steels. As for the stainless steels, the film formed on the

Preprints (www.preprints.org) | NOT PEER-REVIEWED | Posted: 28 September 2023 doi:10.20944/preprints202309.1931.v1

INCONEL 600 also has a bilayer structure with the Cr_2O_3 [14] enriched inner layer and the outer layer formed essentially by Fe_2O_3 oxide and NiO [37]. Other studies suggest that nickel oxide would be present in that structure as $Ni(OH)_2$ [37, 47]. With the increase of the immersion time, the diameter of the capacitive arc of the Nyquist diagrams (Figures 4A and 4B) is increased for both stainless steels. However, the values of the resistors R_2 greater for AISI 316 represented in tables 3 and 4 show that the films formed on AISI 316 are more protective than those formed on AISI 304 in alkaline media. This difference between the two stainless steels is due to the presence of molybdenum in the chemical composition of AISI 316 stainless steel, which promotes a more stable and protective chromium oxide enrichment [38].

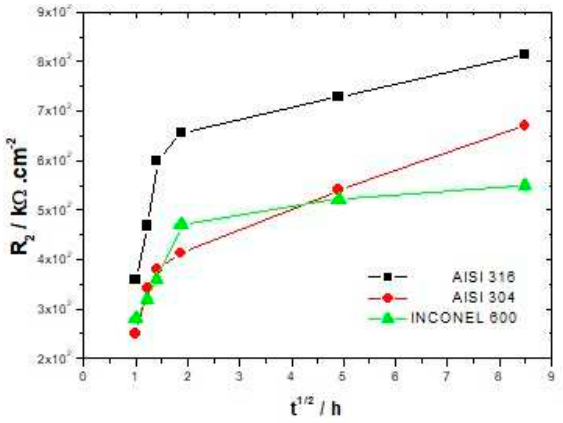

Figure 6. Evolution of the resistance of the film R_2 as a function of immersion time.

In figure 6, it can be seen that the resistance R_2 attributed to the film increases continuously up to 72 hours of immersion for both stainless steels. The INCONEL 600 displays a strong increase in R_2 during the first hours of immersion and beyond 3h30 this increase becomes smoother. It appears therefore that the formation of a stable passive film is faster on INCONEL 600 than on stainless steels. This may be due to the fact that the films formed on the nickel base alloys are thinner than those formed on the stainless steels [37, 48]. However, the values of R_2 (table 3, 4, 5) and the Nyquist figures indicate that the films formed on INCONEL 600 in alkaline environments and at ambient temperature do not appear to be more protective than those formed on stainless steels. On the contrary, it seems that the films formed on AISI 316 are more protective in this alkaline environment.

3.2.2. Atomic Force Microscopy.

Preprints (www.preprints.org) | NOT PEER-REVIEWED | Posted: 28 September 2023 doi:10.20944/preprints202309.1931.v1

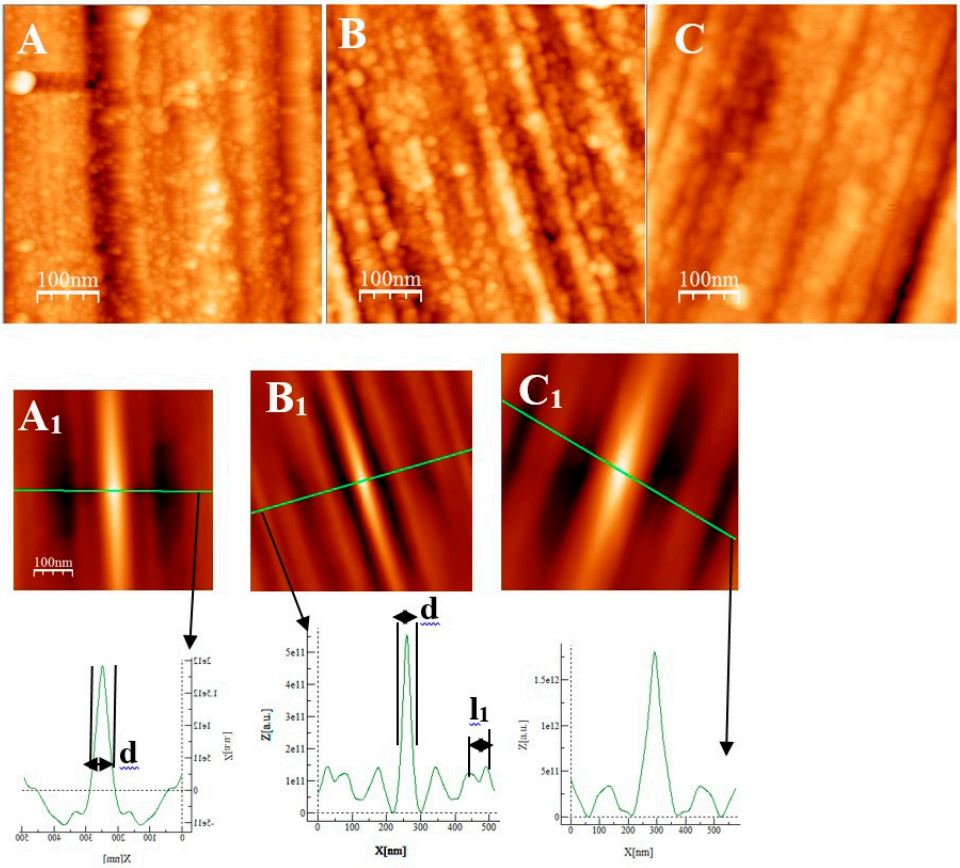

Figure 7. AFM images (500 nm µmx 500 nm) of passive films grown on AISI 304 substrates after polishing as a function of immersion time. (A) ½ h, (B) 3 h ½, (C) 72 h. (A1), (B1) and (C1) are self-correlation images calculated using respectively images A, B and C as input with typical cross-sections allowing to determine a periodicity named l_1 and the mean oxide grain diameter d.

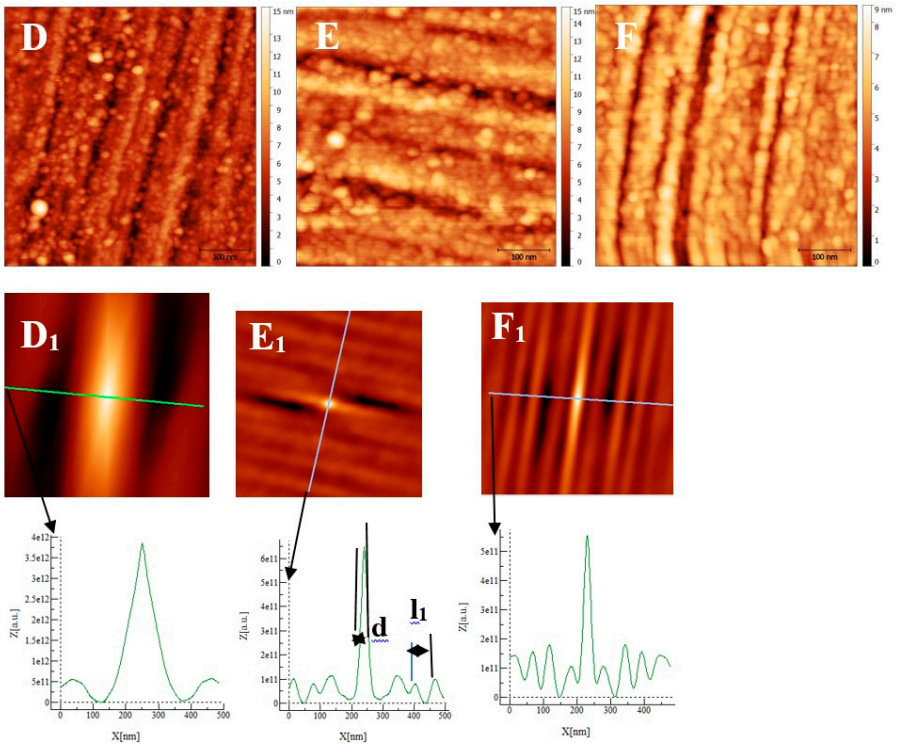

Preprints (www.preprints.org) | NOT PEER-REVIEWED | Posted: 28 September 2023 doi:10.20944/preprints202309.1931.v1

Figure 8. AFM images (500 nm x 500 nm) of passive films grown on AISI 316 substrates after polishing as a function of immersion time. (D) ½ h, (E) 3 h ½, (F) 72 h. (D1), (E1) and (F1) are self-correlation images calculated using respectively images E, D and F as input with typical cross-sections allowing to determine a periodicity named l_1 and the mean oxide grain diameter d.

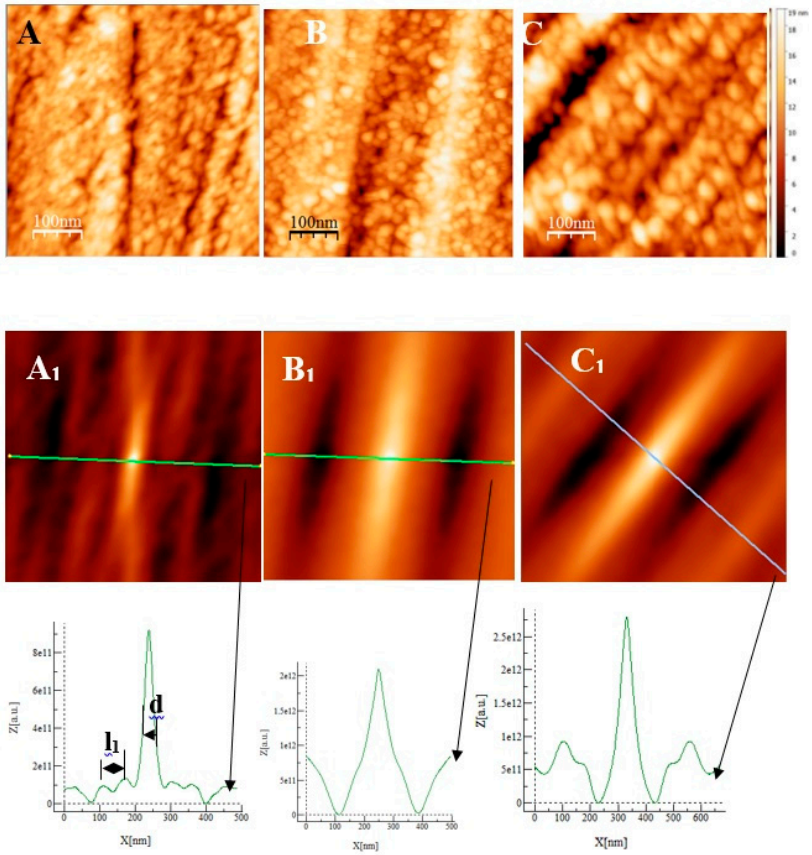

Figure 9. AFM images (0.5 μm x 0.5 μm) of the passive film grown on INCONEL 600 substrates after polishing (Figure 1C) as a function of immersion time: (A) ½ h, (B) 3 h ½, (C) 72 h. (A1), (B1) and (C1) are self-correlation images calculated using respectively images A, B and C as input with typical cross-sections allowing to determine a periodicity named l_1 and the mean oxide grain diameter d.

Some AFM images (500nm × 500 nm) of the passive films formed on the polished substrates (see fig 1for memory of the bare substrate) as a function of the immersion time in an alkaline solution simulating reinforced concrete (NaOH at pH = 13) are given on figure7, figure8 and figure 9 for stainless steels AISI 304 and AISI 316 and INCONEL 600 samples respectively. On Figures 7A and 8D, representing the surfaces of the stainless steels after 30 minutes immersion, polishing grooves can be observed and the first stage of passivation which consists in the formation of small circular oxide grains distributed over the entire active surface and growing along trenches due to the polishing steps. The size of these grains increases with the immersion time until coalescence at t= 3h1/2 which can be seen on the AFM images (figures 7B and 8E). Coalescence generates the covering of the whole surface and the growth became less and less visible. On the surface of INCONEL 600 we do not observe the same behavior as for stainless steels. Indeed, on the figure 9A which represents the surface INCONEL 600 after t = 1/2 h immersion, polishing grooves are less visible than for stainless steels because the oxide film is may be thicker. We noticed that the small oxide structures do not have a well-defined shape on the entire surface. As for AISI 304 and 316 at an immersion time of t = 3h1/2, INCONEL 600 shows the formation of oxide grains that covers its entire surface (Fig 9 B). To quantify these observations, we determine the Root Mean Square (RMS) surface roughness parameter for the different immersion times using the following expression [49].

Preprints (www.preprints.org) | NOT PEER-REVIEWED | Posted: 28 September 2023 doi:10.20944/preprints202309.1931.v1

$$RMS\sqrt{\left(\frac{\sum_{i=1}^{512}\sum_{j=1}^{512}h^2{}_{ij}}{512^2}-\langle\eta\rangle^2\right)} \quad (6)$$

Where $\langle\eta\rangle$ is the mean height of the height distribution $h_{ij}(i,j)$.

Figure 10 shows the variation of the RMS roughness as a function of the square root of the immersion time. The square root of time was used only out of better data presentation matter. For all three alloys, the RMS value increases at t = 1/2 h consistent with the value of the bare substrate and decreases until reaching a minimum at t = 1h for the AISI 316 and INCONEL 600 and at t = 3h1/2 for the AISI 304. At longer immersion times, the roughness increases again for the three alloys, for the AISI 316 a maximum is reached at t = 24h then will decrease until t = 72h. The decrease of the RMS for INCONEL 600 is between t = 3h1 / 2 and t = 24h after, the RMS seems to be constant. For the three alloys, when the immersion time is low, it is reasonable to say that the RMS is may be controlled by the surface roughness of the baresubstrate. On the surface of stainless steels (Fig 7 A and 8D) we observe the formation of small oxide grains isolated on the entire surface that will promote the increase of RMS at t = 1/2 h. We noticed that the size of these grains is much smaller than the ones observed in Y. Li et al's work [26] on carbon steels. With the expansion of immersion time in the alkaline solution, the grain size will tend to increase until coalescence (Fig 7 B and 8E), this will cause the RMS decline. This decrease results from the fact that the size of the grains increases progressively with the time of immersion, causing a covering of the trenches. So, the oxide film has thickened. The influence of the substrate is then lost and the RMS parameter is essentially controlled by the future growth of the passive film.

Unlike stainless steels, the INCONEL 600 at t = 1/2 h (Fig 9A) shows a porous film which covers entirely the substrate. This film is constituted of oxide grains of larger size and round or elongated shapes. When the immersion time reaches t = 3h 1/2, the same characteristics are found as for the stainless steels, the presence of round oxide grains that develop until they reach coalescence. The film obtained covers the polishing grooves and the effect of the substrate on the RMS becomes less important. At immersion times of t = 24h and t = 72h, the RMS is almost identical and polishing scratches are less and less visible (Fig 9C). According to the literature [9], this can be due to the thickening of the oxide film with increasing immersion time. Thanks to figure 10 and the above discussion, we can determine a coalescence time of the oxide grains, noted t_{coal}, corresponding to the immersion time where the RMS reaches a minimum before increasing again and corresponds to a substrate completely covered by an oxide layer that can act as an efficient barrier against corrosion. This affirmation will be confirmed by the SKPFM measurements (section 3.2.3). For Inconel 600 and AISI316 substrates, we obtain the same value of t_{coal} = 60min.For AISI304, t_{coal}=210 min is a little more longer than for the two other substrates. Moreover, the roughness of the oxide formed on INCONEL 600 evolves slowly after 24 hours of immersion. The results of the AFM measurements seem to confirm those obtained by EIS and the analysis of Fig 3. C that shows that the Nyquist diagrams obtained at t = 24h and t = 72h are almost identical. The value of the resistance R_2 of the film was found to be almost identical to the one measured at t=24h and t=72h. There is therefore a correlation between electrochemical impedance measurements and the morphology modification of the oxide surface. To get a better inside on the growth mode of the oxide islands on the trenches of the several substrates, we calculate again the self-correlation function images of each topographic image on figures 7,8 and 9. We can extract from these images two characteristic lengths. Since we observe a periodicity in the cross-sections (see Fig 7A_1, B_1, C_1, fig 8D_1, E_1, F_1 and fig9A_1, B_1, C_1), we determine a periodicity l_1. The width of the central peak at half-maximum taken in the direction of the periodicity give us access to the mean diameter d of the oxide grains. In fact, since clearly the islands grow and coalesce first in the direction perpendicular to the periodicity which corresponds to parallel trenches due to the polishing steps, we can determine only a mean diameter in the direction of the periodicity. In the perpendicular direction the oxide islands are contiguous since the density of nucleation centers for oxide islands is so important on the trenches so that for an immersion time shorter or equal to 30 min (see image A of figure 7), the diameter of an island is great enough to allow the overlapping of neighbors islands along each trenches. The results for l_1 and d as a function of immersion time for the

Preprints (www.preprints.org) | NOT PEER-REVIEWED | Posted: 28 September 2023 doi:10.20944/preprints202309.1931.v1

three substrates using self-correlation images like that of fig 7 and 8 (not all images showed) are given on Table 6.

Table 6. Periodicity l_1 and mean oxide grain diameter d as a function of immersion time for the three substrates, as deduced from self-correlation function images calculations (for examples see Figures 7, 8 and 9 and related cross-sections). The time t=0 corresponds to the bare substrate after the polishing steps and l to the mean distance between two trenches as determined on Figure 1.

	Immersion time(min)						
Samples	0	30	60	180	216	1440	4320
AISI304	l =193±20 nm	l_1=180±10nm d=32±5 nm	l_1=170±20nm d=75±5 nm	l_1=280±10nm d=90±10 nm	No periodicity d=100±10 nm	No periodicity d=110±10 nm	No periodicity d=110±10 nm
AISI316	l =83±15 nm	l_1=90±10nm d=100±10 nm	l_1=100±10nm d=72±5 nm	l_1=180±10nm d=85±5 nm	No periodicity d=90±5 nm	No periodicity d=95±5 nm	No periodicity d=100±5 nm

As can be deduced from the evolution of d and l_1 with the immersion time, the growth mechanism is always the same whatever the substrates is : first oxide islands grow on trenches acting as source for nucleation centers. In this case, the mean diameter d is smaller than the average distance l between trenches and so we observe a periodicity l_1 that corresponds to l. So, the bare substrate remains visible in the topography image. At immersion times lower than 30 min, the oxide islands are separated and coalescence along the trenches occurs at t = 30 min(see image A fig7 and fig9 for example).At this time the mean diameter d is large enough and the density of nucleation great enough to allow the neighboring islands to touch each other conducting to lines of islands separated by a periodicity l_1 equal to l. Afterwards the mean diameter d increases and remains lower than l/2.At an immersion time corresponding to t_{coal} as determined previously, the oxide islands coalescence also in the direction of the periodicity because d became near to l/2.At this time, we notice experimentally that l_1 became 2xl, showing that the growth remains under the influence of the substrate polishing steps. It is only after an immersion time longer and equal to 3h that the periodicity l_1 disappear and the growth is not more under the control of the trenches that means under the control of the bare substrate topography. Afterwards, d increases slowly. The only difference between samples is that coalescence in the direction perpendicular to the trenches occurs at a longer immersion time for AISI316 than for AIS304 and Inconel600 samples, as observed on the RMS roughness variations as a function of immersion time (Figure10).

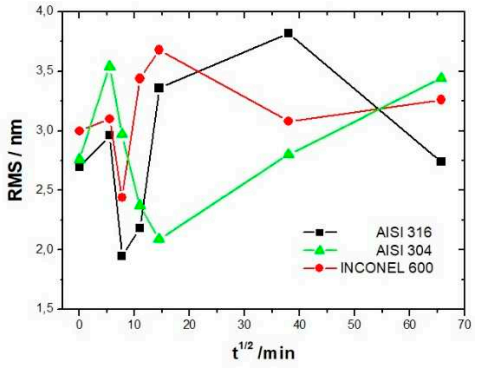

Figure 10. Evolution of the RMS roughness as a function of immersion time for the AISI304, AISI316 and Inconel600 samples.

3.2.3. SKPFM measurements.

Preprints (www.preprints.org) | NOT PEER-REVIEWED | Posted: 28 September 2023 doi:10.20944/preprints202309.1931.v1

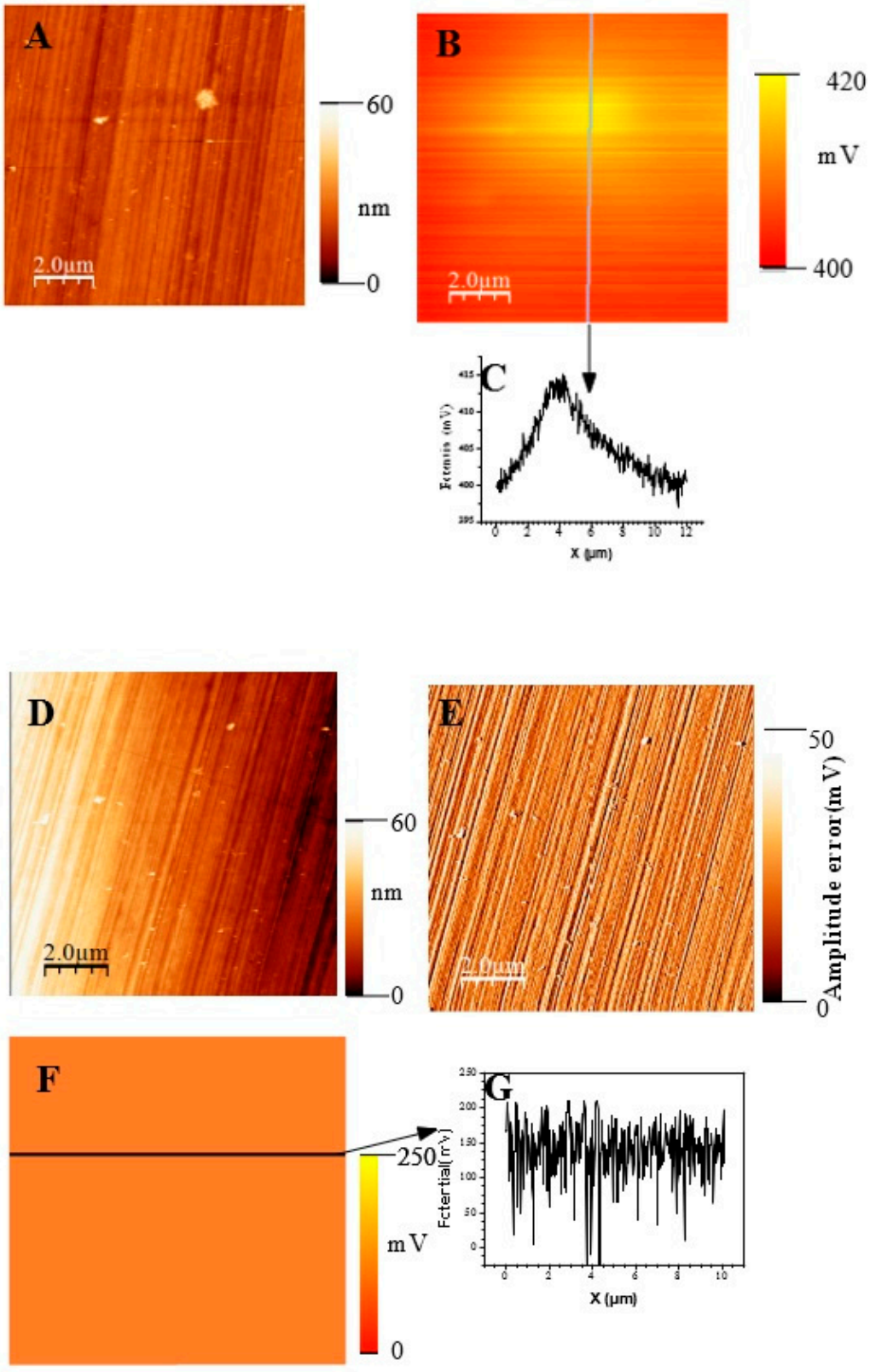

Preprints (www.preprints.org) | NOT PEER-REVIEWED | Posted: 28 September 2023 doi:10.20944/preprints202309.1931.v1

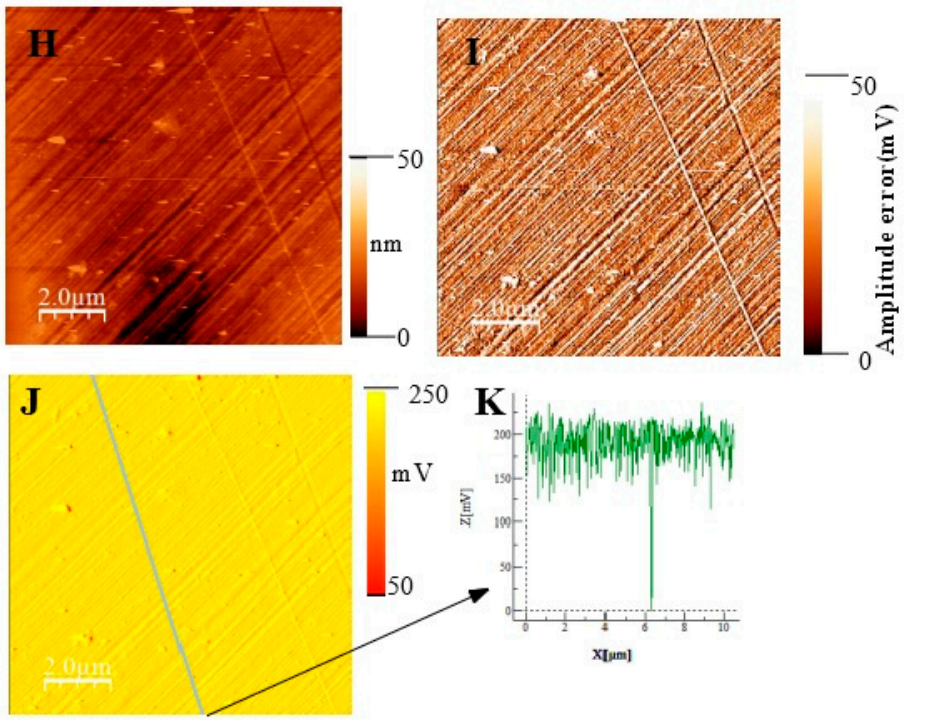

Figure 11. (Large scale (10 µm x 10 µm) topographic AFM and corresponding SKPFM images for three different immersion times measured for the AISI316sample.

t = 30 min (A) surface topography; (B) potential image(SKPFM) associated to image (A);(C) Cross-section along the line showed on image B showing the potential variation across the potential image.t= 1h 30. (D) surface topography; (E)) AFM error image associated to image D; (F) potential image(SKPFM) associated to image (D);(G) Cross-section along the line showed on image F showing the potential variation across a mean value for the potential image. t= 72h (H) surface topography; (I)) AFM error image associated to image H; (J) potential image(SKPFM) associated to image (H);(K) Cross-section along the line showed on image J showing the potential variation across a mean value for the potential image.

Figure 11 show topographic AFM and SKPFM potential images of native films grown on AISI316 at three selected immersion times: at t = ½ h (before coalescence), at t = 3½ h (oxide islands coalescence) at t = 72 h (the native film is complet). Notice that AFM and SKPFM images are tacken taken simultaneously at the same place. As can be seen on the potential images (F, J) and contrarily to thermally grown oxide layers [21], we observe that the surface potential is very homogeneous over the entire analyzed surface (size: 10 µm x 10 µm) since only a very weak spatial variation around a mean value of the surface potential (less than 10 mV) was observed for native films grown on AISI316 and for all immersion times. This result is clearly highlighted on by the different sections (figures 11G, 11K, respectively) along the lines of potential images 11F and 11J respectively. The same results (a very weak spatial variation around a mean value of the surface potential) are obtained for Inconel 600 as for AISI 404 304 samples. And so we can plot the mean value of the surface potential as a function of immersion time as shown on figure 12E,D,F for the three substrates. As explained in the literature, SKPFM techniques give a direct access to the work function difference between the sample surface and the tip. By taking some care, this technique allows therefore a chemical analysis of the surface composition at the micrometric scale. The results of surface potential measurements as a function of the square of immersion time ($t^{½}$) are shown on figure 12 for all substrates. In every case, clearly the bare substrate has the much higher potential (410 mV for AISI304 and AISI316, 920 mV for Inconel 600) and the formation of the first small oxide grains at t = ½ h conduct to an important decrease of this value until coalescence is reached. Afterwards, the potential increases again reaching a maximum of 360 mV (320 mV for AISI316) at t = 24 h and decreasing slowly to 250 mV at t = 72 h for AISI304.For AISI316, the maximum is reached later at t =4h and the potential decrease and

Preprints (www.preprints.org) | NOT PEER-REVIEWED | Posted: 28 September 2023 doi:10.20944/preprints202309.1931.v1

stabilize around 200 mV. The potential evolution is different for Inconel 600 since after coalescence, the potential stabilizes more faster than for AISI304 and AISI316 to a mean value around 250 mV.

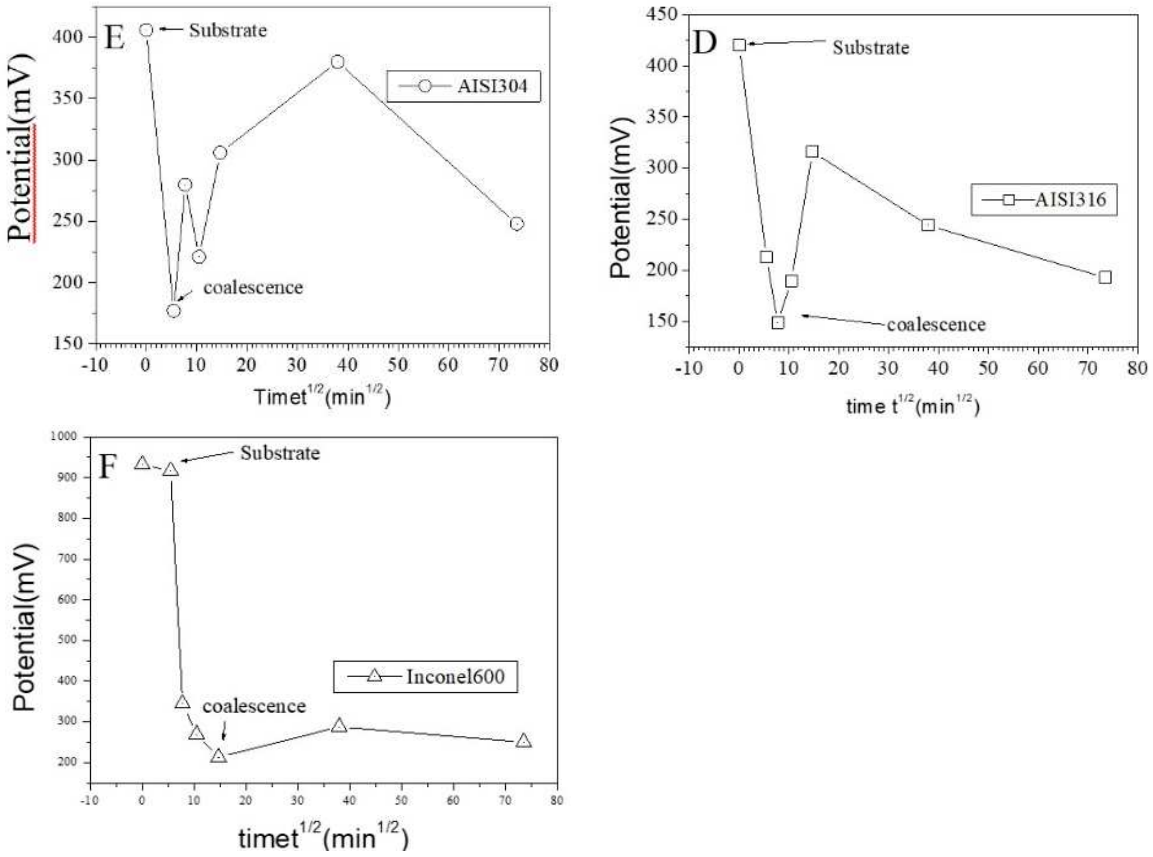

Figure 12. Evolution of the mean surface potential as a function of the square of immersion time ($t^{½}$) for the AISI304(E), AISI316(D) and Inconel600(F) samples.

Our interpretation is based on the results published in references [50, 51] and the actual knowledge concerning the passive layer growth, namely that the highest observed Volta potential in our images corresponds to a chromium enriched phase on the surface. Chromium and iron rich phase are present simultaneously in the layer with an inner chromium oxide layer in contact with the metallic substrate and an outer iron oxide layer in contact with the electrolyte. Let us also remember that the surface potential images probe only the first nanometer of the sample surface in the case of stainless steel and Inconels. So, at t = ½ h, it is probably iron oxide that grow on the surface conducting to the observed important decrease of potential towards the substrate potential. Afterwards, chromium oxide forms at the metallic surface and the potential increase reaching a maximum. At coalescence (t = 3 h ½for AISI304 and Inconel600), the film became continuous and chromium oxide is progressively covered by iron oxide that grows at the electrolyte/film interface conducting to a decrease of the potential until t = 72 h.

Therefore SKPFM measurements are coherent with the AFM observation and EIS results. In fact, AFM data show that the film became continuous after t = 3h ½ which correspond to the time where the shape of the Nyquist diagram is changing. Obviously a very thin passive layer (here not more than few nanometers as estimated by AFM) is enough thick to be an efficient barrier against corrosion since SKPFM images and potential measurements show that the p-n heterojunction [21, 52] consisted by the outer n-type iron oxide and the inner p-type chromium oxide is formed at t = 72 h. The spatially very homogeneous potential at every immersion time show that the chemical composition of the passive layer is very homogenous contrary to the behavior of thermally grown oxide layers where chromium oxide phase continues to be present in contact with the electrolyte until layer thicknesses like 30 nm [21], acting therefore as corrosion centers. In fact, a localized disappearance of one of the

two p-n layers and thus of the junction make corrosion possible which is not the case here after 72 h of immersion.

5. Conclusions

This work focused on the passivation of stainless steels (AISI 304 and AISI 316) and INCONEL 600 in an alkaline solution that simulates reinforced concrete at room temperature. The films are formed by cyclic voltammetry and under natural conditions (OCP). The results obtained show:

1) The films formed by CV are thicker for AISI 304 than for AISI 316 and INCONEL 600. The determination of the residual current density in the passivation zone showed that the films formed on the three alloys are protective. However, the presence of molybdenum in the chemical composition of AISI 316 enables the formation a film that is more stable and more resistant to ion transport. Impedance measurements confirm these results.
2) EIS measurements have shown that the resistance of spontaneously formed films increases with immersion time for all three alloys. As with CV-formed films, AISI 316 also seems to be the alloy that forms the most resistant film. The film formed on INCONEL 600 becomes stable faster than those formed on stainless steels. However, the electrochemical measurements did not show a better protection for the film formed on INCONEL 600 under these experimental conditions.
3) The AFM measurements shows that the growth of the oxide film is under the control of the bare substrate topography and roughness until an immersion time is reached where coalescence occurs. The coalescence time is different as a function of the substrates. After coalescence, the small oxide grains develop on the entire surface of the three substrates a stable homogeneous film that becomes more and more protective with increasing immersion time. This layer is also chemically very homogeneous as shown by SKPFM images. The passive layer is therefore an efficient barrier against corrosion. We have clearly highlighted the correlation between EIS measurements and topographic modifications.

Author Contributions: Conceptualization, Nasreddine Moulayat and Jean Luc Bubendorff; Methodology, Noureddine Benaioun, Nasreddine Moulayat, Noureddine Hakiki and Jean Luc Bubendorff; Validation, Noureddine Benaioun and Jean Luc Bubendorff; Formal analysis, Noureddine Benaioun, Kouider Driss Khodja and Jean Luc Bubendorff; Investigation, Noureddine Benaioun, Hanene Ramdane, Emmanuel Denys, Alban Florentin, Kouider Driss Khodja, Mohamed Heireche and Jean Luc Bubendorff; Resources, Emmanuel Denys, Alban Florentin and Kouider Driss Khodja; Data curation, Hanene Ramdane and Mohamed Heireche; Writing – original draft, Noureddine Benaioun and Jean Luc Bubendorff; Writing – review & editing, Noureddine Benaioun and Jean Luc Bubendorff; Supervision, Nasreddine Moulayat, Noureddine Hakiki and Jean Luc Bubendorff; Project administration, Nasreddine Moulayat and Jean Luc Bubendorff; Funding acquisition, Noureddine Hakiki and Mohamed Heireche.

Acknowledgments: The authors are grateful to the French–Algerian exchange and research program Tassili (Project code CMEP no. 10MDU801), to the "Conseil Général du Haut-Rhin" and to the "Région Alsace now named "Grand Est" and to both universities they belong too, for the financial support (PhD and researchers grants) of this work. .

Conflicts of Interest: The authors declare no conflict of interest.

References

1. S. Joiret, M. Keddam, X. R. Novoa, M. C. Pérez, C. Rangel, H. Takenouti, Cement and Concrete Comp. 24 (2002) 7-15.
2. G. Sahoo, R.Balasubramaniam, Corros. Sci, 50 (2008) 131-143.
3. T. Wu, X. Lu, Z. Chen, X. Feng, Y. Zhang, X. Chen, N. Zhuang, Corros. Sci, 198 (2022): 110102.
4. R.G. Duarte, A.S. Castela, R. Neves, L. Freire, M.F. Montemor, Electrochim. Acta. 124 (2014) 218-224.
5. C. Andrade, M. Keddam, X.R. Novoa, M.C. Perez, C.M. Rangel, H. Takenouti, Electrochim. Acta. 46 (2001) 3905-3912.
6. S. Chakri, I. Frateur, M. E. Orazem, E. M. M. Sutter, T. T. M. Tran, B. Tribollet, V. Vivier, Electrochim. Acta. 20 (2017) 924-930.
7. L. Freire, X. R. Novoa, M.F. Montemor, Chem. Phys. 114 (2009) 962-972.
8. X. Feng, T. Wu , J-l. Luo, X. Lu, Cement and Concrete Composites 112 (2020) 103651
9. D.Addari, B.Elsner, A.Rossi, Electrochim.Acta. 53 (2008) 8078-8086.
10. X.Yuan,X.Wang, Y.Cao,H.Yang, J. Mater. Res. Technol. 2020;9(6)12378-12390.

11. P. Monnartz, Iron-chromium alloys with special consideration of resistance to acids, Metallurgie. 8 (1911) 161.
12. J. Shi, M. Li, M. Wu, J. Ming, Corrosion Science 190 (2021) 109669.
13. Y. Zhang, X. Zhang, S. Chen, J. Liu, T.Li,L. Wang, K. Wu, Corrosion Communications 9 (2023) 77–88.
14. F. Mechehoud, N.E. Benaioun, N.E. Hakiki, A. Khelil, L. Simon, J.L. Bubendorff, Appl. Surf. Sci. 433 (2018) 66-75.
15. S. Haupt, H.H. Strehblow, Langmuir. 3 (1987) 873-885.
16. E. Sosa, R. Cabrera-Sierra, M. T. Oropeza, F. Hernández, N. Casillas, R. Tremont, I. González, Electrochim. Acta. 47 (2003) 1665-1674.
17. S. Haupt, H.H. Strehblow, Corros. Sci. 29 (1989) 163-182.
18. P. Schmutz, D. Landolt, Corros. Sci. 41 (1999) 2143-2163.
19. N.E. Hakiki, M. Da Cunha Belo, J. Electrochem. Soc. 143 (1996) 3088-3094.
20. N.E. Hakiki, S. Boudin, B. Rondot, Corros. Sci. 37 (1995) 1809-1822.
21. B. Maachi, C. Pirri, A. Mehdaoui,N.E. Hakiki, J.L. Bubendorff, Corros. Sci. 53 (2011) 984-991.
22. R. D. Armstrong, K. Edmondson, Electrochim. Acta. 18 (1973) 937-943.
23. C. Chao, L. Lin, D.D. Macdonald, J . Electrochem. Soc. 129 (1982) 1874-1879.
24. J. Hubrecht, M. Embrechts, W. Bogaerts, Electochim. Acta. 38 (1993) 1867-1875.
25. M. Sánchez-Morenoa, H. Takenouti, J.J. García-Jarenoc, F. Vicente, C. Alonso, Electrochim. Acta 54. (2009) 7222-7226.
26. L. Freire, M.J. Carmezima, M.G.S. Ferreira, M.F. Montemor, Electrochim. Acta. 55 (2010) 6174-6181.
27. D.D. Macdonald, Electrochim. Acta. 51 (2006) 1376-1388.
28. L. Veleva, M. A. Alpuche-Aviles, M. K. Graves-Brook, D. O. Wipf, J. Electroanal. Chem. 537 (2002) 85-93.
29. Y. Li, Y. F. Cheng, Applied Surface Science. 396 (2017) 144-153.
30. C. M. Abreu, M. J. Cristobal, X. R. Novoa, G. Pena, M. C. Perez, Electrochim. Acta. 47 (2002) 2215-2222.
31. L. Aigouy, Y. De. Wilde, C.Frétigny, 'Les nouvelles microscopies. A la découverte du nanomonde', Belin (2006).
32. W. Melitz, J. Shen, A. C. Kummel, S. Lee, Surface Science Reports. 66 (2011)1-27.
33. G. Binning, C. F. Quate, C.H. Gerber, Atomic force microscope, Phys. Rev. Lett. 56 (1986) 930.
34. L. Freire, M.A. Catarino, M.I. Godinho, M.J. Ferreira, M.G.S. Ferreira, A.M.P. Simões, M.F. Montemor, Cem. Concr. Compos. 34 (2012) 1075-1081.
35. C.M. Abreu, M.J. Cristobal, R. Losada, X.R. Novoa, G. Pena , M.C. Perez, J. Electroanal. Chem. 572 (2004) 335-345.
36. C.M. Abreu, M.J. Cristobal, R. Losada, X.R. Nóvoa, G. Pena, M.C. Pérez, Electrochim. Acta. 49 (2004) 3049-3056.
37. C.M. Abreu, M.J. Cristobal, R. Losada, X.R. Nóvoa, G. Pena, M.C. Pérez, Electrochim. Acta. 51(2006) 2991-3000.
38. X. Shang, Y. Zhang, N. Qu, X. Tang, Int. J. Electrochem. Sci., 11 (2016) 5870-5876.
39. M. Sánchez, H. Mahmoud, M. C. Alonso, J. Solid. State. Electrochem. 16 (2012) 1193-1202.
40. H. Luo, H. Su, C. Dong, X. Li, Applied Surface Science. 400 (2017) 38-48.
41. A. Pardo, M.C. Merino, A.E. Coy, F. Viejo, R. Arrabal, E. Matykina, Cor. Sci. 50 (2008) 1796-1806.
42. D. Marijan, M. Vukovic, Materials Science Forum, 289 (1998) 1091-1102.
43. M. E. G. Lyons, M. P Brandon, Int. J. Electrochem. Sci. 3 (2008) 1386-1424.
44. J. Kubisztal, A. Budniok, International Journal of Hydrogen Energy. 33 (2008) 4488-4494.
45. L. Freire, M. J. Carmezima, M. G. S. Ferreiraa, M. F. Montemor, Electrochim. Acta. 56 (2011) 5280-5289.
46. J.L. Trinstancho-Reyes, M. Sanchez-Carrillo, R. Sandoval-Jabalera , V.M Orozco- Carmona, F.Almeraya-Calderón, J.G Chacón-Nava, JG Gonzalez-Rodriguez, A. Martínez-Villafañe, Int. J. Electrochem. Sci., 6 (2011) 419 – 431.
47. O. Lavigne, T. Shoji, Y. Takeda, Nucl. Eng. Des. 273 (2014) 435-439.
48. L. A. S. Ries, M. Da Cunha Belo, M. G. S. Ferreira, Cor. Sci.50 (2008) 676-686.
49. Technical note of the AFM manufacturer (Veeco society). The used formula is one of the mathematical definitions of RMS surface roughness.
50. N. E. Benaioun, I. Maafa, A. Florentin, E. Denys, N. E. Hakiki, N. Moulayat, J. L. Bubendorff Appl. Surf.Sci. 436 (2018) 646-652.
51. N. Sathirachinda, R. Pettersson, J. Pan, Corros. Sci. 51 (2009) 1850–1860.
52. N.E. Hakiki, M. Da Cunha Belo, A.M.P. Simoes, M.G.S. Ferreira, J. Electrochem. Soc. 145 (1998) 3821–3829.